Motion Artifact Suppression in Impedance Pneumography Signal for Portable Monitoring of Respiration: An Adaptive Approach

Sardar Ansari, *Member, IEEE*, Kevin R. Ward, and Kayvan Najarian, *Senior Member, IEEE*

***Abstract*—The focus of this paper is motion artifact (MA) reduction from the impedance pneumography (IP) signal, which is widely used to monitor respiration. The amplitude of the MA that contaminates the IP signal is often much larger than the amplitude of the respiratory component of the signal. Moreover, the morphology and frequency composition of the artifacts may be very similar to that of the respiration, making it difficult to remove these artifacts. The proposed filter uses a regularization term to ensure that the pattern of the filtered signal is similar to that of respiration. It also ensures that the amplitude of the filter output is within the expected range of the IP signal by imposing an ε-tube on the filtered signal. The adaptive ε-tube filter is 100 times faster than the previously proposed nonadaptive version and achieves higher accuracies. Moreover, the experimental results, using several different performance measures, suggest that the proposed method outperforms popular MA reduction methods such as normalized least mean squares (NLMS) and recursive least squares (RLS) as well as independent component analysis (ICA). When used to extract the respiratory rate, the adaptive ε-tube achieves a mean error of 1.27 breaths per minute (BPM) compared to 4.72 and 4.63 BPM for the NLMS and RLS filters, respectively. When compared to the ICA algorithm, the proposed filter has an error of 1.06 BPM compared to 3.47 BPM for ICA. The statistical analyses indicate that all of the reported performance improvements are significant.**

***Index Terms*—Epsilon-tube, impedance pneumography (IP), motion artifact (MA), portable and in-home monitoring, respiration monitoring.**

I. Introduction

THE impedance pneumography (IP) signal has been widely used to monitor respiration. It is noninvasive and easy to collect, which makes it suitable for portable monitoring of respiration. Several studies have introduced devices that use the IP signal for portable monitoring of respiration [1]–[5]. These devices can be used to monitor patients with different conditions including chronic obstructive pulmonary disease (COPD) [6], asthma [7], sleep disorders such as obstructive sleep apnea [2], [3] and wheezing disorder [8] as well as continuous measurement of pulmonary flow and tidal volume [9], [10]. Impedance pneumography operates by injecting a low-amplitude high-frequency current into a segment of interest and measuring the voltage gradient between the electrodes. The computed impedance, when measured on the upper body, correlates with respiration. However, the IP signal is highly susceptible to motion artifact (MA), which is mainly caused by the sliding of the electrodes along with the skin [5], [9], [11], [12]. As a result, it is necessary to develop MA reduction methods to improve the practicality of portable monitoring of respiration using the IP technology.

The authors have previously proposed a nonadaptive approach for MA reduction from the IP signal [13]. This paper proposes an adaptive filter that can be used in real time to remove the MA, which is 100 times faster and achieves higher levels of accuracy than the nonadaptive version. In particular, the proposed filter is designed to remove high-amplitude low-frequency artifacts from a relatively periodic IP signal. The amplitude of the artifact can be several times larger than the amplitude of the signal, making it difficult to use conventional MA reduction methods to remove them. The filtering method that is introduced in this paper applies a ε-tube (εT), used in the support vector regression algorithm [14], to the signal to restrict the amplitude of the filtered signal and reconstructs the signal using the periodic characteristic of respiration.

Several methods have been proposed to reduce the effect of MA on other physiological signals such as electrocardiogram (ECG) and photoplethysmography (PPG) signals. However, only a handful of studies exist that address the problem of MA reduction in the IP signal. For example, the authors in [11] and [15]–[17] studied the type and the number of the electrodes that are used and their placements. Other works, including [18] and [19], have studied the effect of measuring the IP signal with different frequencies. However, to our knowledge, no practical signal processing or machine learning methods have been proposed to overcome the problem.

The signal processing methods that are proposed to remove MA from the ECG and PPG signals can be mainly divided into two categories. The first category uses independent component analysis (ICA) and principal component analysis to estimate

Manuscript received August 26, 2015; revised December 21, 2015; accepted January 27, 2016. Date of publication February 3, 2016; date of current version March 3, 2017.

S. Ansari and K. R. Ward are with the Department of Emergency Medicine, University of Michigan, Ann Arbor, MI 48105 USA (e-mail: sardara@med.umich.edu; keward@med.umich.edu).

K. Najarian is with the Department of Computational Medicine and Bioinformatics, University of Michigan, Ann Arbor, MI 48109 USA (e-mail: kayvan@med.umich.edu).

This paper has supplementary downloadable material available at http://ieeexplore.ieee.org.

Digital Object Identifier 10.1109/JBHI.2016.2524646

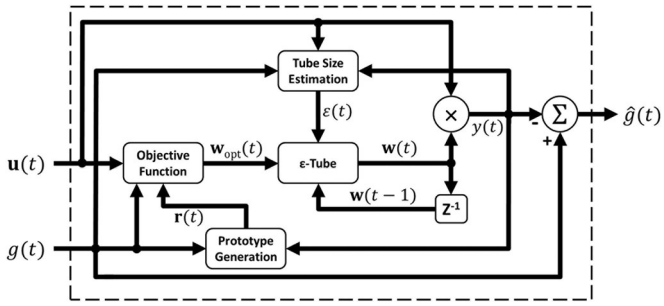

Fig. 1. Block diagram of the A-εT filter with the input IP signal values, $g(t)$, the vector of accelerometer signal values, $\mathbf{u}(t)$, and the filtered IP signal $\hat{g}(t)$.

MA as an independent source of variation in the signal [20]–[24]. These methods require at least two readings of the signal from two different locations. For the ECG signal, this does not impose a major restriction since multichannel acquisition of the ECG signal is commonly available, which is not the case for the IP signal. Moreover, the independence assumption is violated in this case, e.g., walking or running can affect the respiratory pattern, making it dependent on the maneuver.

The second category of MA reduction methods uses different adaptive filtering methods, such as least mean squares (LMS) [25]–[30], recursive least squares (RLS) [31]–[33], normalized LMS (NLMS) [34], [35], and normalized signed regressor LMS [36]. Despite their popularity, adaptive filters cannot use the information that is available regarding the pattern of the signal, such as the periodic property of the respiratory signal. Moreover, adaptive filters can also adapt to the signal of interest and treat it as noise when the MA and the signal are similar in shape and frequency. In particular, low *forgetting factor* values, which allow the filter to effectively respond to rapid changes in the signal that are caused by MA, would also result in the filter adapting to the sinusoidal patterns of the IP signal and eventually treating them as MA. However, the adaptive εT (A-εT) filter that is introduced in this paper has a mechanism to make that distinction, and therefore, it only models the MA and not the respiratory component of the signal.

Other methods that have been used for MA reduction include Kalman filter [37], [38], Widrow's adaptive noise cancellation [39], singular value decomposition [40], Fourier series analysis [41], filter banks and matched filters [42], smoothed pseudo Wigner–Ville distribution [43], and wavelet transform [44].

The next section discusses the details of the proposed filter. Section III introduces the data collection and preprocessing of the signals and Section IV discusses the results of the comparisons between the proposed filter and the currently existing ones. Finally, Section V discusses the implications of the reported results and Section VI presents the concluding remarks and the potential future works.

II. Methods

The block diagram of the proposed filter is shown in Fig. 1. The filter is composed of an objective function that finds the optimal filter coefficients $\mathbf{w}_{\text{opt}}(t)$ by minimizing the error between the frequency components of the filtered signal inside a sliding window and a frequency prototype, $\mathbf{r}(t)$, that is computed from the previous windows. These coefficients are then fed into a block that applies the εT constraints to the filter output to ensure that the amplitude of the filtered signal falls within the tube. The filter also contains two components that compute the frequency prototype and adjust the size of the tube, ε.

This section starts by introducing the preliminary concepts that are used in the rest of the paper. Then, the details of each component of the block diagram are presented.

A. Preliminaries

In this paper, matrices and vectors are denoted by bold upper and lower case letters, respectively. Also, all the vectors are column vectors and all the indices start from 0. The ith row and the jth column of a matrix $\mathbf{A}$ are denoted by $\mathbf{A}^{i,\cdot}$ and $\mathbf{A}^{\cdot,j}$, respectively, and $\mathbf{a}^i$ indicates the ith element of vector $\mathbf{a}$.

The idea of using the εT for MA reduction was first introduced in [45]. It was later expanded and improved by using an autoregressive exogenous model instead of the tangent sigmoid activation functions in order to increase the flexibility of the MA reduction method [13]. The A-εT filter that is introduced here is a finite impulse response (FIR) filter and uses a tube to constrain the amplitude of the filtered signal at time t, i.e.

$$|g(t) - \mathbf{w}^{\mathrm{T}}(t)\mathbf{u}(t)| \leq \varepsilon(t) \tag{1}$$

where $g(t)$ is the value of the IP signal and $\varepsilon(t)$ is the width of the tube, both at time t, $\mathbf{u}(t)$ is a $3n_b \times 1$ vector of three-axis accelerometer measurements from $t - n_b + 1$ to t, $\mathbf{w}(t)$ is a $3n_b \times 1$ vector of the filter coefficients and n_b is the filter order.

The constraint in (1) reduces the size of the search space for the filter coefficients to a large extent. Additionally, a second criterion is used to choose the best set of coefficients inside the reduced search space. Assuming that the impedance signal follows a regular pattern, the periodicity of the signal can be used as a measure for regularity. A perfectly regular signal is one with a frequency composition that is invariant along the time dimension. This property can be measured using the Stockwell transform (S-transform) of the signal [46]. S-transform is a generalization of the short time Fourier transform that provides a time–frequency representation of the signal and is very sensitive to irregularities. A regular signal would have an S-transform for which the frequency decomposition remains nearly constant as time advances. The S-transform is applied to a sliding window which is centered at the sample that is being processed. This leads to a delay in the filter output that is equal to the length of a half window (typically around 3 s).

A sample window and the related quantities are shown in Fig. 2. The portion of the IP signal that is inside the window is denoted by $\mathbf{g}(t)$ and is partitioned as $[\mathbf{g}_1(t)^{\mathrm{T}}|\mathbf{g}_2(t)^{\mathrm{T}}]^{\mathrm{T}}$ where $\mathbf{g}_1(t) = [g(t-T+1), g(t-T+2), \ldots, g(t-1)]^{\mathrm{T}}$ and $\mathbf{g}_2(t) = [g(t), g(t+1), \ldots, g(t+T)]^{\mathrm{T}}$. The vector of the filter outputs in the first half of the window (past samples before t) and the estimated MA in the second half of the window (present and future samples) are denoted by $\mathbf{y}(t)$ and $\mathbf{z}(t)$, respectively. The input vectors from t to $t+T$ are collected in matrix $\mathbf{U}(t)$ where the ith row is $\mathbf{u}(t+i-1)$. Moreover, $p \in [t-T+1, t+T]$ and $n \in [0, N-1]$ are the time and frequency indices for the

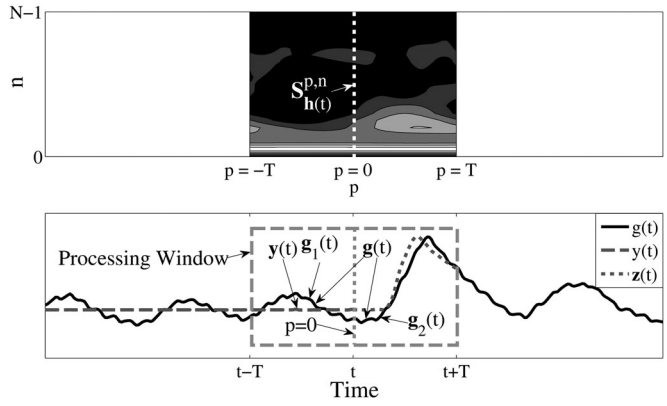

Fig. 2. Sample window (bottom) and its S-transform (top) of length $2T$, stretching from $t-T+1$ to $t+T$, and t in the center of the window. Notice that $\mathbf{g}$, $\mathbf{g}_1$, $\mathbf{g}_2$ and $\mathbf{y}$ are bold on the graph (i.e., they are vectors) while $g(t)$ and $y(t)$ in the legend are not (i.e., they are scalars).

S-transform, respectively, where N is the number of frequency components. Note that $p=0$ in the S-transform domain (the frequency components in the middle of the window) correspond to time t in the time domain. The S-transform is applied to $\mathbf{h}(t)$, which is the vector of the filtered signal from $t-T+1$ to $t+T$, first half of which is composed of the IP signal minus the filter outputs up to $t-1$, and the second half is the IP signal minus the estimates for MA, i.e.

$$\begin{aligned}\mathbf{h}(t) &= \mathbf{g}(t) - \begin{pmatrix}\mathbf{y}(t)\\ \mathbf{z}(t)\end{pmatrix} = \begin{pmatrix}\mathbf{g}_1(t)\\ \mathbf{g}_2(t)\end{pmatrix} - \begin{pmatrix}\mathbf{y}(t)\\ \mathbf{z}(t)\end{pmatrix}\\ &= \begin{pmatrix}\mathbf{g}_1(t)-\mathbf{y}(t)\\ \mathbf{g}_2(t)\end{pmatrix} - \begin{pmatrix}\mathbf{0}_{T\times 1}\\ \mathbf{z}(t)\end{pmatrix} = \mathbf{h}_1(t) - \mathbf{h}_2(t) \quad (2)\end{aligned}$$

where

$$\mathbf{h}_1(t) = \begin{pmatrix}\mathbf{g}_1(t)-\mathbf{y}(t)\\ \mathbf{g}_2(t)\end{pmatrix}, \quad \mathbf{h}_2(t) = \begin{pmatrix}\mathbf{0}_{T\times 1}\\ \mathbf{z}(t)\end{pmatrix} \quad (3)$$

and

$$\mathbf{z}(t) = \mathbf{U}(t)\mathbf{w}(t). \quad (4)$$

The S-transform of $\mathbf{h}(t)$, denoted by $\mathcal{S}^{p,n}_{\mathbf{h}(t)}$, can be computed as

$$\mathcal{S}^{p,n}_{\mathbf{h}(t)} = \mathcal{S}^{p,n}_{\mathbf{h}_1(t)} - \mathcal{S}^{p,n}_{\mathbf{h}_2(t)} \quad (5)$$

and the frequency components at $p=0$ can be found as

$$\begin{aligned}\mathcal{S}^{0,\cdot}_{\mathbf{h}(t)} &= \mathcal{S}^{0,\cdot}_{\mathbf{h}_1(t)} - \mathcal{S}^{0,\cdot}_{\mathbf{h}_2(t)} = \mathcal{S}^{0,\cdot}_{\mathbf{h}_1(t)} - \sum_{k=0}^{T}\mathbf{z}^k(t)\mathcal{S}^{0,\cdot}_{\delta(x-k)}\\ &= \mathcal{S}^{0,\cdot}_{\mathbf{h}_1(t)} - \mathbf{M}_\delta\mathbf{z}(t) \quad (6)\end{aligned}$$

where $\delta(x-k)$ is a delta functions with argument $x\in[-T+1, T]$ that is shifted by k samples, and $\mathbf{M}_\delta$ is a matrix whose ith column is $\mathcal{S}^{0,\cdot}_{\delta(x-i+1)}$. The estimated value for the MA at time t is the first element of $\mathbf{z}$, i.e.

$$y(t) = \mathbf{z}^0(t) = \mathbf{w}^{\mathrm{T}}(t)\mathbf{u}(t). \quad (7)$$

The proposed filter computes a prototype, $\mathbf{r}(t)$, for the frequency components at $p=0$ at time $t-T+1$, $\mathcal{S}^{0,\cdot}_{\mathbf{h}(t-T-1)}$. This prototype represents the frequency components of a periodic waveform that is expected to be present in the signal. It is computed based on the previously observed processing windows and automatically adapts to the changes in the morphology of the waveform. The complexity of $\mathbf{r}(t)$ is fixed in advance so that it remains unaffected in the presence of MA. The prototype, which will be further discussed in Section II-D, is used to measure the regularity of the filtered signal.

In the rest of this paper, Re[·] and Im[·] represent the real and imaginary parts of a complex number. Also, the time index t is dropped for simplicity where it is appropriate.

B. Objective Function

The objective function of the A-εT filter is composed of two terms

$$\text{Minimize}(\mathbf{r}-\mathcal{S}^{0,\cdot}_{\mathbf{h}})^{\mathrm{T}}\overline{(\mathbf{r}-\mathcal{S}^{0,\cdot}_{\mathbf{h}})} + \frac{\gamma}{q}\mathbf{w}^{\mathrm{T}}\mathbf{w} \quad (8)$$

where γ is a design parameter and q is a nonnegative nondecreasing function of the power of the deviations of the IP signal from the tube. It is computed within the processing window and is discussed at the end of this section. The first term minimizes the squared error between the frequency components of the filtered signal in the middle of the window (at $p=0$) and the prototype $\mathbf{r}(t)$. The second term minimizes the norm of the coefficient vector. The filter gives a smaller weight to the second term when MA is present, giving more flexibility to the coefficients in $\mathbf{w}$ to grow. On the other hand, when MA is absent, the second term becomes dominant, ensuring that the filter avoids modeling the respiratory component of the signal, which results in a stable output from the filter.

Minimizing the objective function in (8) is equivalent to optimizing the following function:

$$\begin{aligned}\text{Minimize } f = \; & 2\text{Re}[(\mathbf{r}-\mathcal{S}^{0,\cdot}_{\mathbf{h}_1})^{\mathrm{T}}\mathbf{C}_1^{\mathrm{T}}]\mathbf{U}\mathbf{w}\\ & + \mathbf{w}^{\mathrm{T}}\left(\mathbf{U}^{\mathrm{T}}\mathbf{C}_2\mathbf{U} + \frac{\gamma}{q}\mathbf{I}\right)\mathbf{w} \quad (9)\end{aligned}$$

where $\mathbf{C}_1 = \mathbf{M}_\delta^{\mathrm{H}}$, $\mathbf{C}_2 = \mathbf{M}_\delta^{\mathrm{T}}\overline{\mathbf{M}_\delta}$ are constant matrices and $\mathbf{M}_\delta^{\mathrm{H}}$ is the Hermitian transpose of $\mathbf{M}_\delta$. The derivation of (9) is provided in Appendix A. The objective function in (9) is a quadratic form in terms of $\mathbf{w}$, and $\mathbf{U}^{\mathrm{T}}\mathbf{C}_2\mathbf{U} + \frac{\gamma}{q}\mathbf{I}$ is positive semidefinite. Consequently, f is a convex quadratic program with a unique optimal solution $\mathbf{w}_{\text{opt}}(t)$ at time t

$$\begin{aligned}\mathbf{w}_{\text{opt}}(t) = \; & -(\mathbf{U}^{\mathrm{T}}(t)\mathbf{C}_2\mathbf{U}(t) + \frac{\gamma}{q(t)}\mathbf{I})^{-1}\mathbf{U}^{\mathrm{T}}(t)\text{Re}[\mathbf{C}_1(\mathbf{r}(t)\\ & -\mathcal{S}^{0,\cdot}_{\mathbf{h}_1(t)})] \quad (10)\end{aligned}$$

when $q(t)>0$, and $\mathbf{w}_{\text{opt}}(t)=0$ when $q(t)=0$. The latter ensures that the signal is not altered by the filter when the tube is not violated. After finding $\mathbf{w}_{\text{opt}}(t)$, the vector of coefficient updates will be equal to

$$\mathbf{w}_\Delta(t) = \mathbf{w}_{\text{opt}}(t) - \mathbf{w}(t-1). \quad (11)$$

The filter coefficients should also abide by the constraints, forcing the amplitude of the filtered signal to fall within the tube. The method for enforcing the εT constraints is discussed in the next section.

As mentioned earlier, $q(t)$ is a nonnegative nondecreasing function of the power of the deviations of the IP signal from the tube, where deviation is defined as $e(t) = \max(g(t) - \varepsilon(t), -g(t) - \varepsilon(t), 0)$. Then, $q(t)$ can be found using

$$q(t) = \left[\frac{1}{2T} \sum_{i=t-T+1}^{t+T} e(i)^2 \right]^{1/2}. \tag{12}$$

The design parameter γ, adjusts the balance between the first and second terms in the objective function. A small value for γ would result in a more flexible filter that can quickly adapt to the changes in the IP signal caused by MA. On the other hand, a larger value leads to a more stable filter and prevents the filter from diminishing the respiratory component of the signal by modeling its periodic pattern. The optimal value for γ depends on the amplitudes of the IP and accelerometer signals, which are determined by the electrode types, amplification levels, and parameters of the sensing devices.

Equation (10) involves $\mathcal{S}^{0,\cdot}_{\mathbf{h}_1(t)}$ that requires the S-transform of $\mathbf{h}_1(t)$ to be computed in every update. This is a time-consuming operation; hence, we propose an alternative method in Appendix B to compute $\mathcal{S}^{0,\cdot}_{\mathbf{h}_1(t)}$ more efficiently.

Next section will discuss the constraints, which ensure that the amplitude of the filtered signal falls within the tube.

C. Constraints

The A-εT filter ensures that the amplitude of the filtered signal is bounded. The following constraints enforce this restriction in the middle of the processing window.

$$\begin{aligned} -\mathbf{u}^{\mathrm{T}}(t)\mathbf{w}(t) + g(t) + \varepsilon(t) \geq 0 \\ \mathbf{u}^{\mathrm{T}}(t)\mathbf{w}(t) - g(t) + \varepsilon(t) \geq 0. \end{aligned} \tag{13}$$

A modified version of the Rosen's gradient projection method [47] is used to enforce the constraints in (13). For the time being, it is assumed that the filter coefficients $\mathbf{w}(t-1)$ satisfy (13). The left-hand side of the constraints can be expressed in the matrix form as

$$\mathbf{v} = \mathbf{A}\mathbf{w} - \mathbf{b} \tag{14}$$

where

$$\mathbf{A} = \begin{pmatrix} -\mathbf{u}^{\mathrm{T}}(t) \\ \mathbf{u}^{\mathrm{T}}(t) \end{pmatrix}, \quad \mathbf{b} = \begin{pmatrix} -g(t) - \varepsilon(t) \\ g(t) - \varepsilon(t) \end{pmatrix}. \tag{15}$$

The conventional gradient projection method forms a matrix $\mathbf{N}$ whose columns are the gradients of the active constraints at $\mathbf{w}(t-1)$. A constraint is active if it holds at equality. The gradient projection method is based on projecting the desired search direction, $\mathbf{w}_\Delta(t)$, onto the space that is tangent to the boundaries of the active constraints. In other words, the result of this projection, $\mathbf{d}$, is the closest vector to $\mathbf{w}_\Delta(t)$ whose direction points along the boundaries of the active constraints. Unlike static optimization problems where the objective surface is fixed, the objective function in (9) varies with time; hence, a modified version of gradient projection method is used that allows for the active constraints to become inactive, i.e., it allows departure from an active constraint if $\mathbf{w}_\Delta(t)$ points toward the feasible region of that constraint. This can be done by forming $\mathbf{N}$ such that it only includes the active constraints for which

$$(\mathbf{A}^{i,\cdot})^{\mathrm{T}}\mathbf{w}_\Delta(t) \leq 0, \quad i = 1, 2. \tag{16}$$

If no such constraint exists, the update vector $\mathbf{d}$ will be the same as $\mathbf{w}_\Delta(t)$; otherwise, $\mathbf{d}$ can be found using

$$\mathbf{d} = (\mathbf{I} - \mathbf{N}(\mathbf{N}^{\mathrm{T}}\mathbf{N})^{-1}\mathbf{N}^{\mathrm{T}})\mathbf{w}_\Delta(t). \tag{17}$$

It is noteworthy that the two constraints in (13) are parallel, i.e., they are never active at the same time. As a result, the size of $\mathbf{N}^{\mathrm{T}}\mathbf{N}$ is no more than 1×1. Hence, the inverse in (17) reduces to a scaler one. Moreover, the filter reaches the global minimum for the constrained optimization program with a single gradient descent step. The appropriate update from $\mathbf{w}(t-1)$ to $\mathbf{w}(t)$ is of the form

$$\mathbf{w}(t) = \mathbf{w}(t-1) + \alpha\mathbf{d} \tag{18}$$

where α is the step length. The ith constraint imposes a bound on $\mathbf{d}$ if

$$(\mathbf{A}^{i,\cdot})^{\mathrm{T}}\mathbf{d} < 0 \tag{19}$$

and hence, α should be chosen to avoid violating that constraint by

$$\alpha = \min\left(\frac{-(\mathbf{A}^{i,\cdot})^{\mathrm{T}}\mathbf{w}(t-1) + \mathbf{b}^i}{(\mathbf{A}^{i,\cdot})^{\mathrm{T}}\mathbf{d}}, 1 \right). \tag{20}$$

Using the aforementioned equation, $\mathbf{w}(t-1) + \alpha\mathbf{d}$ either reaches the global minimum of the objective function or hits one of the constraints.

The modified gradient projection method explained above assumes that $\mathbf{w}(t-1)$ satisfies the constraints in (13). These constraints depend on the accelerometer signals $\mathbf{u}(t)$ which vary with time; hence, the coefficient vector $\mathbf{w}(t-1)$ might become infeasible at time t. As a result, $\mathbf{w}(t-1)$ needs to be corrected such that it conforms to the constraints before it is used in (11) and (18) by

$$\mathbf{w}(t-1) \leftarrow \mathbf{w}(t-1) + \mathbf{d}_{\mathrm{c}} \tag{21}$$

where $\mathbf{d}_{\mathrm{c}}$ is the correction vector. At most one of the constraints can be violated at a time. If the ith constraint is violated, i.e., $\mathbf{v}^i < 0$, the update vector can be computed as

$$\mathbf{d}_{\mathrm{c}} = -\mathbf{N}(\mathbf{N}^{\mathrm{T}}\mathbf{N})^{-1}\mathbf{A}^{i,\cdot}. \tag{22}$$

It is enough to perform the correction step in (21) once with a step size of one. This step needs to be performed before we compute $\mathbf{w}_\Delta(t)$ using (11).

D. Prototype

The prototype should be built based on the intrinsic characteristics of the input signal $g(t)$. In this case, the IP signal has two major components, a dominant respiratory component and a secondary heart rate component. The aim of this paper is to extract the respiratory component of the IP signal. Therefore, we use a piecewise linear approximation of the squared magnitude of the frequency components in the middle of the

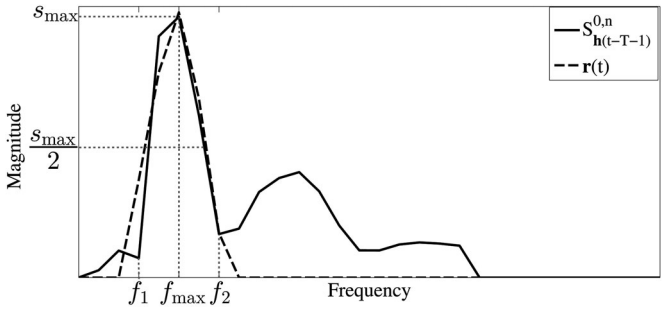

Fig. 3. Amplitude of a sample slice of the S-transform at $p = 0$, $|\mathcal{S}^{0,.}_{\mathbf{h}(t-T-1)}|$, along with the amplitude of the corresponding prototype, $|\mathbf{r}(t)|$. The y-axis is the magnitude of the frequencies.

window from $t - 2T - 1$ to $t - 1$, $|\mathcal{S}^{0,.}_{\mathbf{h}(t-T-1)}|^2$, to build a prototype for the respiratory component of the signal. An instance of $|\mathcal{S}^{0,.}_{\mathbf{h}(t-T-1)}|$ and the corresponding piecewise linear approximation are shown in Fig. 3. In order to compute $\mathbf{r}(t)$, we first find the most dominant frequency component, $f_{\max}$, whose amplitude is denoted by $s_{\max}$. Next, the closest frequencies before and after $f_{\max}$, f_1 and f_2, whose amplitudes are smaller than $0.5s_{\max}$, are found. This threshold is chosen intuitively and verified experimentally to create a narrow prototype. For each of the segments from f_1 to $f_{\max}$ and from $f_{\max}$ to f_2, we fit two linear models to approximate $\mathrm{Re}[\mathcal{S}^{0,.}_{\mathbf{h}(t')}]^2$ and $\mathrm{Im}[\mathcal{S}^{0,.}_{\mathbf{h}(t')}]^2$ where $t' = t - T - 1$. Let

$$\mathbf{y}_{r1} = \begin{pmatrix} \mathrm{Re}[\mathcal{S}^{0,f_1}_{\mathbf{h}(t')}]^2 \\ \mathrm{Re}[\mathcal{S}^{0,f_1+1}_{\mathbf{h}(t')}]^2 \\ \vdots \\ \mathrm{Re}[\mathcal{S}^{0,f_{\max}}_{\mathbf{h}(t')}]^2 \end{pmatrix}, \ \mathbf{y}_{i1} = \begin{pmatrix} \mathrm{Im}[\mathcal{S}^{0,f_1}_{\mathbf{h}(t')}]^2 \\ \mathrm{Im}[\mathcal{S}^{0,f_1+1}_{\mathbf{h}(t')}]^2 \\ \vdots \\ \mathrm{Im}[\mathcal{S}^{0,f_{\max}}_{\mathbf{h}(t')}]^2 \end{pmatrix} \quad (23)$$

$$\mathbf{y}_{r2} = \begin{pmatrix} \mathrm{Re}[\mathcal{S}^{0,f_{\max}}_{\mathbf{h}(t')}]^2 \\ \mathrm{Re}[\mathcal{S}^{0,f_{\max}+1}_{\mathbf{h}(t')}]^2 \\ \vdots \\ \mathrm{Re}[\mathcal{S}^{0,f_2}_{\mathbf{h}(t')}]^2 \end{pmatrix}, \ \mathbf{y}_{i2} = \begin{pmatrix} \mathrm{Im}[\mathcal{S}^{0,f_{\max}}_{\mathbf{h}(t')}]^2 \\ \mathrm{Im}[\mathcal{S}^{0,f_{\max}+1}_{\mathbf{h}(t')}]^2 \\ \vdots \\ \mathrm{Im}[\mathcal{S}^{0,f_2}_{\mathbf{h}(t')}]^2 \end{pmatrix} \quad (24)$$

and

$$\mathbf{X}_1 = \begin{pmatrix} 1 & f_1 \\ 1 & f_1+1 \\ \vdots & \vdots \\ 1 & f_{\max} \end{pmatrix}, \ \mathbf{X}_2 = \begin{pmatrix} 1 & f_{\max} \\ 1 & f_{\max}+1 \\ \vdots & \vdots \\ 1 & f_2 \end{pmatrix}. \quad (25)$$

The least-squares approximations for the real and imaginary parts of the two segments can be found as

$$\begin{aligned} \hat{\mathbf{y}}_{r1} &= \mathbf{X}_1(\mathbf{X}_1^{\mathrm{T}}\mathbf{X}_1)^{-1}\mathbf{X}_1^{\mathrm{T}}\mathbf{y}_{r1} \\ \hat{\mathbf{y}}_{i1} &= \mathbf{X}_1(\mathbf{X}_1^{\mathrm{T}}\mathbf{X}_1)^{-1}\mathbf{X}_1^{\mathrm{T}}\mathbf{y}_{i1} \\ \hat{\mathbf{y}}_{r2} &= \mathbf{X}_2(\mathbf{X}_2^{\mathrm{T}}\mathbf{X}_2)^{-1}\mathbf{X}_2^{\mathrm{T}}\mathbf{y}_{r2} \\ \hat{\mathbf{y}}_{i2} &= \mathbf{X}_2(\mathbf{X}_2^{\mathrm{T}}\mathbf{X}_2)^{-1}\mathbf{X}_2^{\mathrm{T}}\mathbf{y}_{i2}. \end{aligned} \quad (26)$$

Then, the final estimates for each of the segments will be computed as

$$\begin{aligned} \mathbf{l}_1 &= \sqrt{\max(\hat{\mathbf{y}}_{r1}, \mathbf{0})} + j\sqrt{\max(\hat{\mathbf{y}}_{i1}, \mathbf{0})} \\ \mathbf{l}_2 &= \sqrt{\max(\hat{\mathbf{y}}_{r2}, \mathbf{0})} + j\sqrt{\max(\hat{\mathbf{y}}_{i2}, \mathbf{0})} \end{aligned} \quad (27)$$

where the *square root* and the *max* are element-wise operators. Then, l_1 and l_2 are combined to form $\mathbf{r}'(t)$

$$\mathbf{r}'(t) = [\mathbf{0}_{1\times(f_1-1)} \quad \mathbf{l}_1'^{\mathrm{T}} \quad \mu \quad \mathbf{l}_2'^{\mathrm{T}} \quad \mathbf{0}_{1\times(N-f_2)}]^{\mathrm{T}} \quad (28)$$

where $\mathbf{l}_1'$ is the same as $\mathbf{l}_1$ excluding its last element, $\mathbf{l}_2'$ is the same as $\mathbf{l}_2$ excluding its first element, and μ is the mean of the last element of $\mathbf{l}_1$ and the first element of $\mathbf{l}_2$. As a result, $|\mathbf{r}'(t)|^2$ is a piecewise linear approximation for $|\mathcal{S}^{0,.}_{\mathbf{h}(t')}|^2$ from f_1 to f_2. Finally, the A-εT filter adjusts the phase of the prototype to match that of $\mathcal{S}^{0,.}_{\mathbf{h}(t)}$ as follows:

$$\mathbf{r}_n(t) = |\mathbf{r}'_n(t)|e^{-j2\pi n(\tau(n)-1)/2T} \quad (29)$$

where $\tau(n)$ is the circular shift associated with frequency n and is defined as

$$\tau(n) = -\frac{T}{\pi n}\phi[\mathcal{S}^{0,.}_{\mathbf{h}(t-1)}]. \quad (30)$$

By shifting the frequency axis such that $f_{\max} = 0$, the second columns in $\mathbf{X}_1$ and $\mathbf{X}_2$ will be composed of consecutive numbers from $f_1 - f_{\max}$ to 0 and from 0 to $f_2 - f_{\max}$, respectively. Therefore, the terms $\mathbf{X}_1(\mathbf{X}_1^{\mathrm{T}}\mathbf{X}_1)^{-1}\mathbf{X}_1^{\mathrm{T}}$ and $\mathbf{X}_2(\mathbf{X}_2^{\mathrm{T}}\mathbf{X}_2)^{-1}\mathbf{X}_2^{\mathrm{T}}$ can be precomputed for different values of f_1 and f_2 and be used throughout the filtering process. As a result, the equations in (26) will reduce to simple matrix multiplications, which would decrease the execution time of the filter.

The filter updates the prototype only when the signal is in a calm state, as defined in the next section. When the signal is contaminated by MA, the filter uses the last prototype that was obtained when the signal was in the calm state. This would prevent the prototype from adapting to the noise that is due to the residual MA after filtering the signal.

E. Tube Size

The amplitude of the IP signal is proportional to the depth of breath. As a result, the filter should be able to accommodate the changes that occur in the amplitude by varying the tube size. Unlike the nonadaptive εT filter, which uses a constant tube size specific to each instance of MA, the A-εT filter updates the tube size adaptively.

In order to detect the MAs, the filter looks at the power of the accelerometer signal within the window, which can be computed as

$$p(t) = \left[\frac{1}{6T}\sum_{i=t-T+1}^{t+T}\mathbf{a}(i)^{\mathrm{T}}\mathbf{a}(i)\right]^{1/2} \quad (31)$$

where $\mathbf{a}(t)$ is the vector of the three-axis accelerometer values. The value of $p(t)$ is compared to a threshold to decide whether the tube size should be updated or not. The threshold is chosen based on the amplitude of the baseline noise present in the

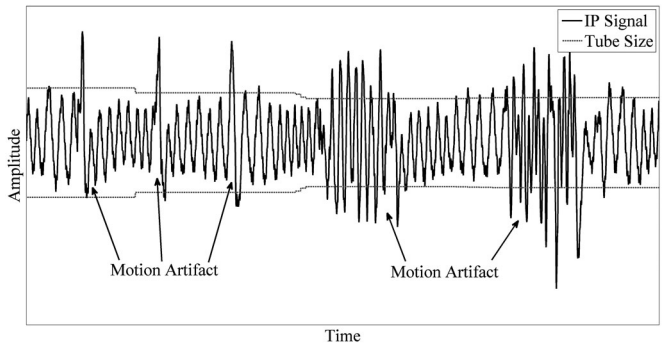

Fig. 4. Sample IP signal and the corresponding tube size.

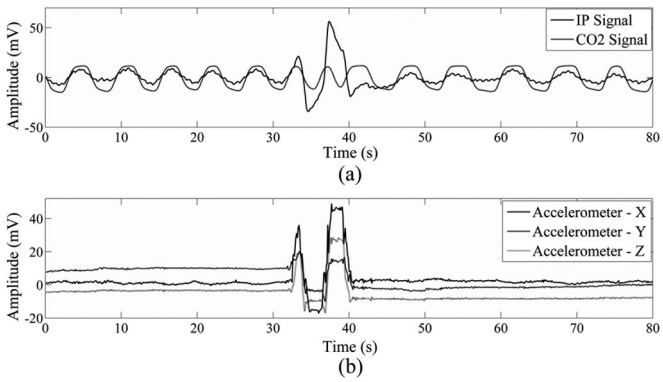

Fig. 5. Sample of the collected signals. (a) Sample of the IP and the $EtCO_2$ signals that are contaminated by the movement of opening the window and (b) Corresponding accelerometer readings.

accelerometer signals, which depends on the hardware that is used.

When the signal is in the calm state and the tube is violated, the filter increases the size of the tube by 1% of the size of the violation. If $g(t)$ does not exceed the tube size, the filter tries to maintain a margin between the signal and the tube in a window that spans from $t - 4T$ to t by setting the tube size to be 10% larger than the maximum amplitude of the signal inside the window. A portion of the IP signal and the resulting tube are shown in Fig. 4.

III. Data Collection and Processing

The data that are used for evaluation is obtained using a Biopac MP150. The IP and end-tidal CO_2 ($EtCO_2$) signals are measured using Biopac EBI100C and CO2100C modules, respectively. The $EtCO_2$ is the amount of CO_2 during exhalation and is used as a reference signal for respiration. Moreover, a three-axis accelerometer module is built and used in the experiments. All the signals are captured at 250 Hz, down-sampled to 10 Hz for processing purposes.

The electrode placements are shown in Fig. 6. The pneumograph's current electrodes are placed between the serratus posterior superior and serratus posterior inferior muscles on the subject's back. The voltage electrodes are placed beside the current electrodes along the path between them. The accelerometer module is placed on the subject's right arm, allowing it to

Fig. 6. Electrode configuration for acquiring the IP signal.

capture the movements of the arm as well as the upper body, both of which have the largest impact on the IP signal. The sensitivity of the accelerometer sensor is chosen such that it captures crude movements that generate MA, but it does not pick up subtle movements that are caused by respiration. This electrode setting is chosen since it is suitable for a portable monitoring device in the form of an armband. Moreover, our experiments indicate that this setting is less susceptible to MA compared to the traditional transthoracic placement. However, the electrode placements need to be investigated more thoroughly, which is outside the scope of this paper.

The proposed A-εT filter is assessed by conducting two experiments. The first experiment compares the proposed filter to nonadaptive εT, NLMS and RLS filters. The latter two are chosen to represent the family of adaptive filters that are popular for MA reduction. The IP and accelerometer signals are collected from a total of 13 subjects. Each subject is asked to perform the maneuvers that are summarized in Table I. Maneuvers 1 to 9 are transient while maneuvers 10 to 14 are periodic. The subjects are in a sitting position during all the maneuvers except maneuvers 7, 8, 13, and 14. Maneuvers 13 and 14 are performed once while all the other maneuvers are conducted about three times. The subjects performed a total of 504 maneuvers during 589.5 min of data collection, 143.9 min of which is contaminated by MA.

The second experiment is conducted to compare the A-εT filter to the ICA algorithm. A total of 273 maneuvers are collected from seven subjects. The total signal collection time and maneuver time are 316.5 and 81.4 min, respectively. The IP

TABLE I
MANEUVERS THAT ARE PERFORMED IN THE EXPERIMENTS

Maneuver	Description
1	Raising the arm and holding it up.
2	Dropping the arm after it was held up for 10 s.
3	Raising the arm and dropping it immediately.
4	Imitating the act of drinking a cup of water.
5	Twisting the upper body towards right and back.
6	Twisting the upper body towards left and back.
7	Standing up.
8	Sitting down after 10 s.
9	Imitating the act of opening a window.
10	Raising the arm and dropping it continuously.
11	Imitating the act of taking food from a plate and putting it in the mouth continuously.
12	Twisting the upper body toward right and left continuously.
13	While standing, walking in place.
14	While standing, running in place.

signals are collected through two simultaneous channels since ICA algorithm requires at least two readings of the input signals. In addition to the setting shown in Fig. 6, the traditional transthoracic electrode placement is used for the second channel. The independent components for the two channels are found by maximizing the non-Gaussianity using the FastICA algorithm.

The signals were filtered using bandpass Butterworth filters before MA removal. The cutoff frequencies used for the accelerometer signals were 0.05 and 2 Hz. The IP signals were bandpass filtered between 0.0005 and 2 Hz in the first experiment and between 0.0005 and 0.5 Hz in the second experiment. The latter was chosen to eliminate the cardiac component of the IP signal, which might appear as a third independent component when ICA is applied to the signal. A sample portion of the IP signal along with the $EtCO_2$ and accelerometer signals are shown in Fig. 5.

Some of the performance measures that are used for comparison are computed based on the extracted respiratory rates from the $EtCO_2$ and filtered IP signals. The respiratory rates are extracted by applying the S-transform to a 30-s long sliding window. The step size is 10 s and the respiratory rate is extracted from the middle 10 s of the window. The dominant frequency between 0 and 2 Hz is considered to be the respiratory rate. A threshold on the amplitude of the dominant frequency is used to detect when the subject is not breathing.

IV. RESULTS

Several different performance measures were used to compare the proposed method against the most popular existing methods for MA reduction. This included the Pearson correlations between the filtered signal and the reference $EtCO_2$ signal, denoted by *corr*. Also, several other measures were computed based on the error between the extracted respiratory rates from the filtered IP signal and the rates extracted from the $EtCO_2$ signal. *Dev1* and *Dev3* are the proportions of times when the error is smaller than 1 and 3 breaths per minute (BPM), respectively. Also, *Mean Err*, *St.D. Err,* and *Max Err* are the averages of mean, standard deviation, and maximum error across different instances of MA, respectively.

The filter parameters for all the methods were chosen using subject-wise cross validation, where one of the subjects was left out for testing in each fold and the parameters were selected to minimize the *Mean Err* for the rest of the subjects. The selected filter parameters for the A-εT filter were $n_b = 5$ and $\gamma =$ 2e-3 in all the folds in both experiments except one of the folds in the first experiment for which the optimal parameters were $n_b = 4$ and $\gamma = 1.5$e-3. The filter order for the NLMS filter was 35 in all the folds while the step size was between 0.05 and 0.1 and leakage parameter was between 0.93 and 0.95. For the RLS filter, the filter order and the forgetting factor were 5 and 0.99 in all the folds, respectively. Finally, the ICA activation functions were chosen to be Gaussian, $u\exp(-au^2/2)$, with $a = 11$ in all the folds.

Fig. 7 illustrates two samples of raw IP signals contaminated by maneuver 6 (transient) and maneuver 10 (periodic), as well as the filtering results using A-εT, NLMS, RLS, and ICA filters. The A-εT filter guarantees that the amplitude of the filtered signal is within the tube. However, the amplitude of the MA residuals is still much larger than the amplitude of the respiratory component after NLMS, RLS, and ICA filters are applied. It is evident from Fig. 7(a2)–(a5) and 7(b2)–(b5) that A-εT filter can effectively remove the MA from the IP signal while NLMS, RLS, and ICA are not successful in doing so. Moreover, the performance of the filtering methods, compared in Table II, indicate that A-εT outperforms all the other methods according to all the performance measures. Furthermore, all the differences are shown to be statistically significant.

Figs. 8 and 9 illustrate the correlations and mean errors for different maneuvers for signals that were filtered using A-εT, εT, NLMS, RLS, and ICA filters. It is evident that the A-εT filter has a better performance compared to the other four methods. Figs. 8(a) and 9(a) indicate that the correlation between the $EtCO_2$ signal and the filtered IP signal is always larger when the A-εT filter is used. Moreover, the A-εT filter achieves a lower *Mean Err* with the exception of maneuver 7.

The A-εT filter achieves a *Mean Err* of less than 2 BPM across all the maneuvers with the exception of maneuver 12 for which the *mean error* is 2.5 BPM. The results are consistent during slow breathing (e.g., maneuver 3) and fast breathing (e.g., maneuver 14) periods. This level of reliability makes the A-εT filter a suitable choice for real-time monitoring of patients in-home and in-hospital.

The supplementary video shows the A-εT filter in action. On the top, it depicts the S-transform of the original signal inside the window and the S-transform of the filtered signal at $t - T - 1$ from which the prototype $\mathbf{r}(t)$ is computed, as well as the magnitude of the frequency components at $p = 0$ and the computed prototype in the center. In the middle section, the video shows the original IP signal and the estimated MA using the A-εT filter. Finally, the bottom part depicts the filtered signal along with the reference $EtCO_2$ signal and the εT margins.

All in all, it can be concluded that the A-εT filter outperforms the NLMS, RLS, and ICA filters. It has a better performance

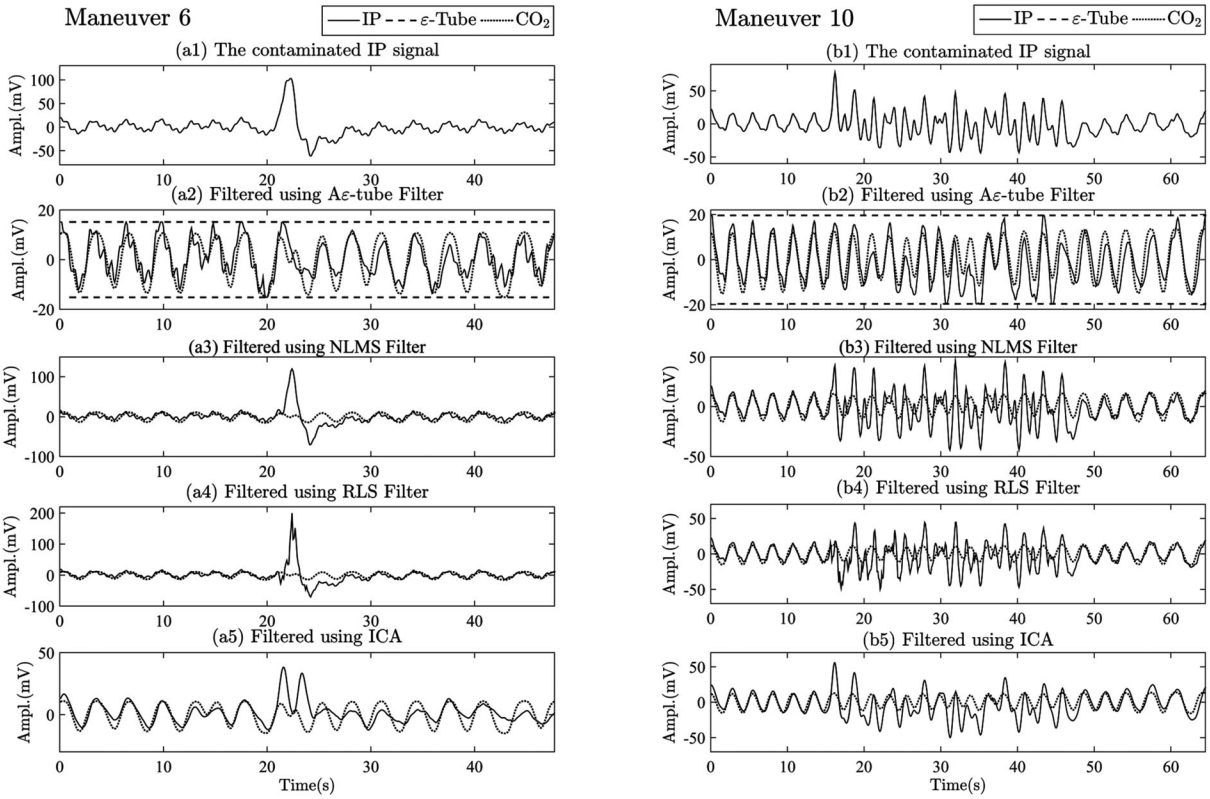

Fig. 7. Two examples of MA before and after filtering are depicted in this figure. Fig. (a1)–(a5) (left column) correspond to an instance of maneuver 6, while an instance of maneuver 10 is shown in (b1)–(b5) (right column).

TABLE II
RESULTS OF THE FIRST EXPERIMENT COMPARING A-εT FILTER VERSUS εTF, NLMS, AND RLS, AS WELL AS THE SECOND EXPERIMENT COMPARING A-εT FILTER VERSUS ICA

Method	Corr	Dev1	Dev3	Mean Err	St.D. Err	Max Err
A-εTF	**0.750**†‡§	**0.745**†‡§	**0.894**†‡§	**1.270**†‡§	**2.067**†‡§	**8.564**†‡§
εTF	0.680	0.690	0.855	1.894	2.784	13.558
NLMS	0.472	0.538	0.680	4.720	4.683	19.759
RLS	0.569	0.621	0.752	4.626	6.017	29.744
A-εTF	**0.786***	**0.784***	**0.921***	**1.061***	**1.915***	**8.488***
ICA	0.672	0.670	0.784	3.468	3.349	11.738

The numbers in bold indicate the best outcomes with respect to each performance measure. In the first experiment, †, ‡, and § denote the statistically significant differences against εTF, NLMS, and RLS, respectively. A Steel-Dwass test (nonparametric version of Tukey's HSD multiple comparisons test) was used that tests the statistical significance of all the differences simultaneously. In the second experiment, a nonparametric Mann–Whitney U test was used and significant differences are marked by *.

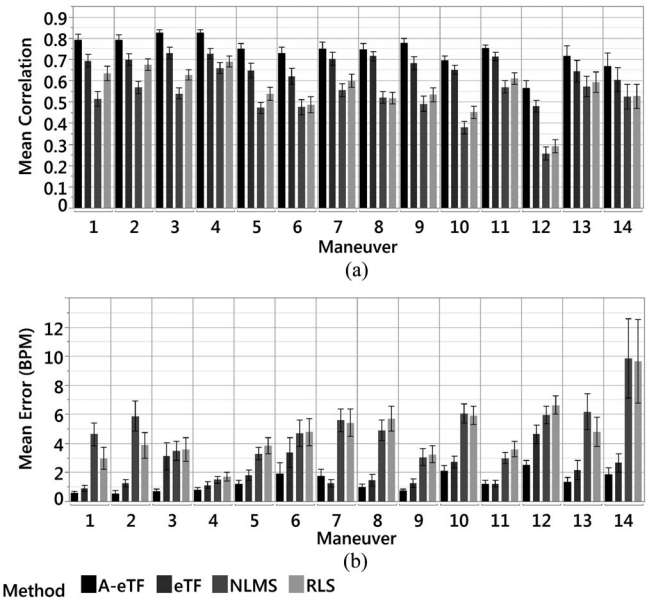

Fig. 8. Results of the first experiment comparing the A-εTF against εTF, NLMS, and RLS for different maneuvers. The bars indicate one standard deviation. (a) Correlations between the filtered signals and the EtCO2 signal, (b) Mean error in the respiratory rates extracted from the filteredsignals and the EtCO2 signal.

than nonadaptive εT filter and it is much more efficient in terms of the execution time and memory usage. In our experiments, conducted on a laptop with a quad-core CPU and 8 GB of memory running MATLAB, the A-εT execution time was 0.422 ms per sample while the nonadaptive εT had an execution time of 41.21 ms per sample. The is because the A-εT filter has a linear computational complexity of $O(n)$, where n is the number of samples in the signal, whereas the nonadaptive εT filter uses the interior-point algorithm to solve a nonlinear constrained optimization problem for each instance of MA which results in a filter with a high computational complexity.

V. DISCUSSION

The advantages and disadvantages of several MA reduction methods are compared in [48]. The proposed A-εT filter

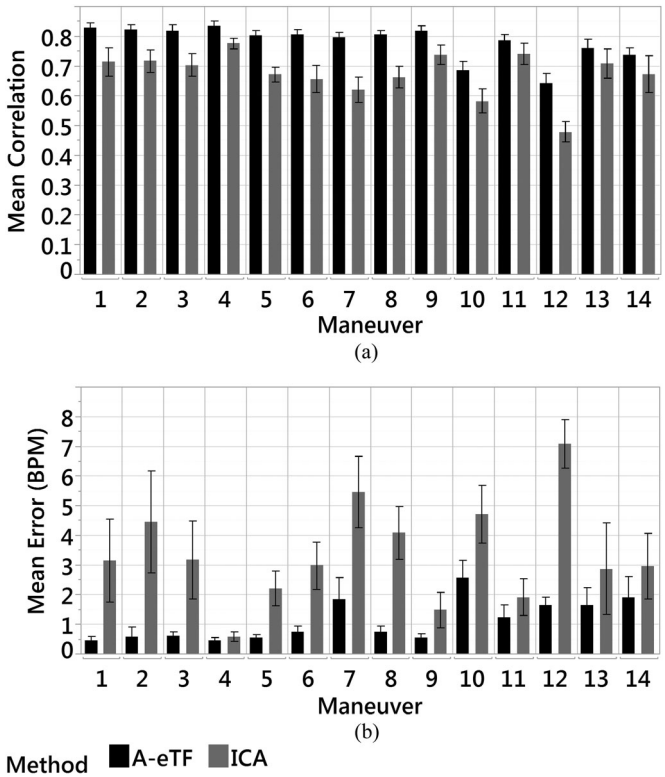

Fig. 9. Results of the second experiment comparing the A-εTF against ICA for different maneuvers. The bars indicate one standard deviation. (a) Correlations between the filtered signals and the EtCO2 signal, (b) Mean error in the respiratory rates extracted from the filteredsignals and the EtCO2 signal.

performs similar to other adaptive filters in terms of the comparison measures that are used in [48], i.e., the filter is fully automated, can operate in real time, on a single channel and in the nonlinear domain, but it requires an additional sensor (accelerometer sensor in this case), and *a priori* information about the sensors and signals is required to set the filter parameters such as γ. The A-εT filter also benefits from additional advantages over conventional methods such as ICA and adaptive filters that are explained in the following.

Several factors contribute to the deficiency of the conventional methods in removing the high-amplitude MAs from the IP signal. For the ICA filter, the statistical independence between the source signals is not guaranteed since the breathing rate can be influenced by subject's movement. As a result, the ICA algorithm is not capable of separating the respiratory and MA components of the signal effectively. Unlike ICA, the A-εT filter does not make any assumptions regarding the independence of different components of the signal.

The conventional adaptive filters have a convergence parameter (forgetting factor for RLS and step size for NLMS) that controls the flexibility of the filter in adapting to recent changes in the signal. The onset of MA causes a sudden change in the amplitude of the signal. Therefore, the convergence parameter should be set to make the filter flexible enough to quickly adapt to these changes. However, a flexible filter will also adapt to less drastic changes associated with respiration. As a result, the RLS and NLMS filters are either too flexible at the cost of modeling both respiration and MA simultaneously, or too "stiff" to quickly react to the onset of MA. This problem is caused by the fact that respiratory component of the signal and MA have similar frequency contents and the amplitude of the MA is much larger than the amplitude of the signal. Unlike these filters, the A-εT filter has a mechanism to distinguish between the low-amplitude respiratory components and the high-amplitude MA by imposing an εT on the signal and "disabling" the filter when MA is not present by changing the balance between the terms in (8).

Unlike our previous work, the A-εT filter works in an adaptive fashion and is about 100 times faster than the εT filter. Moreover, the εT filter is an infinite impulse response (IIR) filter whose objective function is non-convex and has multiple local optima. On the other hand, A-εT is an finite impulse response filter with a convex quadratic objective function that has a unique solution. Furthermore, the A-εT filter has a variable tube size, which adapts to the amplitude of the respiratory component of the IP signal while the εT filter has a constant tube size that is applied to each instance of MA. All in all, the adaptive version of the εT filter is more efficient and effective than the previous nonadaptive version.

VI. Conclusion and Future Works

In this paper, we have proposed a novel filtering method to remove the high-amplitude low-frequency artifacts from the IP signal that are caused by motion. The proposed filter takes advantage of the periodic property of the IP signal by minimizing the error between the filtered signal and a frequency prototype that represents the periodic pattern of the signal. It also imposes an ε-tube on the filter signal to ensure that the amplitude of the filter output is within the expected range. The A-εT filter is shown to be more accurate compared to the NLMS, RLS, and ICA filters and is more effective and less computationally demanding than the previous nonadaptive version.

The A-εT filter can be used in portable monitoring devices that use the IP technology to monitor respiration continuously and noninvasively. Moreover, it can be potentially used to detect several medical conditions such as COPD and sleep apnea. However, the effectiveness of using the A-εT filter in these applications needs to be verified in future studies.

The MA reduction is a common challenge in monitoring other physiological signals as well. The effectiveness of the proposed method in removing the MA from other physiological signals, such as ECG and PPG, can be investigated in the future. To do so, one needs to modify the way the frequency prototypes are generated to represent the dynamics of the signal in question while the rest of the filtering method remains intact. The effectiveness of the modified filter would depend on how accurately the new prototype represents the periodic pattern of the signal. Moreover, the A-εT filter can be compared to other existing methods for MA reduction that are not included in this paper. Furthermore, the effect of different types of electrodes such as textile and textile-integrated sensors, which have been recently used in the wearable devices, on the performance of the proposed filter should be investigated. Finally, the impact of different electrode placements that are suggested in the

literature for portable acquisition of the IP signal on the proposed filtering method can be studied.

APPENDIX A
DERIVATION OF THE OBJECTIVE FUNCTION

The objective function in (8) can be expanded as

$$(\mathbf{r}-\mathcal{S}_{\mathbf{h}}^{0,\cdot})^{\mathrm{T}}(\overline{\mathbf{r}}-\overline{\mathcal{S}_{\mathbf{h}}^{0,\cdot}})+\frac{\gamma}{q}\mathbf{w}^{\mathrm{T}}\mathbf{w}=\mathbf{r}^{\mathrm{T}}\overline{\mathbf{r}}-2\mathrm{Re}[\mathbf{r}^{\mathrm{T}}\overline{\mathcal{S}_{\mathbf{h}}^{0,\cdot}}]$$
$$+(\mathcal{S}_{\mathbf{h}}^{0,\cdot})^{\mathrm{T}}\overline{\mathcal{S}_{\mathbf{h}}^{0,\cdot}}+\frac{\gamma}{q}\mathbf{w}^{\mathrm{T}}\mathbf{w}=\mathbf{r}^{\mathrm{T}}\overline{\mathbf{r}}-2\mathrm{Re}[\mathbf{r}^{\mathrm{T}}\overline{\mathcal{S}_{\mathbf{h}_1}^{0,\cdot}}]$$
$$+2\mathrm{Re}[\mathbf{r}^{\mathrm{T}}\overline{\mathbf{M}_\delta}]\mathbf{z}+(\mathcal{S}_{\mathbf{h}}^{0,\cdot})^{\mathrm{T}}\overline{\mathcal{S}_{\mathbf{h}}^{0,\cdot}}+\frac{\gamma}{q}\mathbf{w}^{\mathrm{T}}\mathbf{w}. \quad (32)$$

The fourth term in (32) can be expressed as

$$(\mathcal{S}_{\mathbf{h}}^{0,\cdot})^{\mathrm{T}}\overline{\mathcal{S}_{\mathbf{h}}^{0,\cdot}}=(\mathcal{S}_{\mathbf{h1}}^{0,\cdot}-\mathbf{M}_\delta\mathbf{z})^{\mathrm{T}}(\overline{\mathcal{S}_{\mathbf{h1}}^{0,\cdot}}-\overline{\mathbf{M}_\delta}\mathbf{z})=(\mathcal{S}_{\mathbf{h1}}^{0,\cdot})^{\mathrm{T}}\overline{\mathcal{S}_{\mathbf{h1}}^{0,\cdot}}$$
$$-\mathbf{z}^{\mathrm{T}}(\mathbf{M}_\delta^{\mathrm{H}}\mathcal{S}_{\mathbf{h1}}^{0,\cdot}+\mathbf{M}_\delta^{\mathrm{T}}\overline{\mathcal{S}_{\mathbf{h1}}^{0,\cdot}})+\mathbf{z}^{\mathrm{T}}\mathbf{M}_\delta^{\mathrm{T}}\overline{\mathbf{M}_\delta}\mathbf{z}=(\mathcal{S}_{\mathbf{h1}}^{0,\cdot})^{\mathrm{T}}\overline{\mathcal{S}_{\mathbf{h1}}^{0,\cdot}}$$
$$-2\mathbf{z}^{\mathrm{T}}\mathrm{Re}[\mathbf{M}_\delta^{\mathrm{H}}\mathcal{S}_{\mathbf{h1}}^{0,\cdot}]+\mathbf{z}^{\mathrm{T}}\mathbf{M}_\delta^{\mathrm{T}}\overline{\mathbf{M}_\delta}\mathbf{z}. \quad (33)$$

Substituting (33) into (32) leads to

$$\mathbf{r}^{\mathrm{T}}\overline{\mathbf{r}}-2\mathrm{Re}[\mathbf{r}^{\mathrm{T}}\overline{\mathcal{S}_{\mathbf{h}_1}^{0,\cdot}}]+2\mathrm{Re}[\mathbf{r}^{\mathrm{T}}\overline{\mathbf{M}_\delta}]\mathbf{z}+(\mathcal{S}_{\mathbf{h1}}^{0,\cdot})^{\mathrm{T}}\overline{\mathcal{S}_{\mathbf{h1}}^{0,\cdot}}$$
$$-2\mathbf{z}^{\mathrm{T}}\mathrm{Re}[\mathbf{M}_\delta^{\mathrm{H}}\mathcal{S}_{\mathbf{h1}}^{0,\cdot}]+\mathbf{z}^{\mathrm{T}}\mathbf{M}_\delta^{\mathrm{T}}\overline{\mathbf{M}_\delta}\mathbf{z}+\frac{\gamma}{q}\mathbf{w}^{\mathrm{T}}\mathbf{w}. \quad (34)$$

The first, second, and fourth terms do not depend on the filter coefficients. Hence, they can be removed from the objective function. After removing these terms and substituting $\mathbf{Uw}$ for $\mathbf{z}$, we get

$$2\mathrm{Re}[\mathbf{r}^{\mathrm{T}}\overline{\mathbf{M}_\delta}]\mathbf{Uw}-2\mathrm{Re}[\mathbf{M}_\delta^{\mathrm{H}}\mathcal{S}_{\mathbf{h1}}^{0,\cdot}]^{\mathrm{T}}\mathbf{Uw}+\mathbf{w}^{\mathrm{T}}\mathbf{U}^{\mathrm{T}}\mathbf{M}_\delta^{\mathrm{T}}\overline{\mathbf{M}_\delta}\mathbf{Uw}$$
$$+\frac{\gamma}{q}\mathbf{w}^{\mathrm{T}}\mathbf{w}=2\mathrm{Re}[(\mathbf{r}-\mathcal{S}_{\mathbf{h1}}^{0,\cdot})^{\mathrm{T}}\overline{\mathbf{M}_\delta}]\mathbf{Uw}$$
$$+\mathbf{w}^{\mathrm{T}}(\mathbf{U}^{\mathrm{T}}\mathbf{M}_\delta^{\mathrm{T}}\overline{\mathbf{M}_\delta}\mathbf{U}+\frac{\gamma}{q}\mathbf{I})\mathbf{w}. \quad (35)$$

In the aforementioned expression, $\overline{\mathbf{M}_\delta}$ and $\mathbf{M}_\delta^{\mathrm{T}}\overline{\mathbf{M}_\delta}$ are constant. Therefore, the final objective function can be expressed as

$$\text{Minimize } f=\ 2\mathrm{Re}[(\mathbf{r}-\mathcal{S}_{\mathbf{h}_1}^{0,\cdot})^{\mathrm{T}}\mathbf{C}_1^{\mathrm{T}}]\mathbf{Uw}$$
$$+\mathbf{w}^{\mathrm{T}}(\mathbf{U}^{\mathrm{T}}\mathbf{C}_2\mathbf{U}+\frac{\gamma}{q}\mathbf{I})\mathbf{w} \quad (36)$$

where $\mathbf{C}_1=\mathbf{M}_\delta^{\mathrm{H}}$ and $\mathbf{C}_2=\mathbf{M}_\delta^{\mathrm{T}}\overline{\mathbf{M}_\delta}$.

APPENDIX B
COMPUTING THE S-TRANSFORM EFFICIENTLY

As time advances from $t-1$ to t, the new S-transform $\mathcal{S}_{\mathbf{h}_1(t)}$ can be generated from $\mathcal{S}_{\mathbf{h}_1(t-1)}$ by taking a few steps. First, the elements of $\mathcal{S}_{\mathbf{h}_1(t-1)}$ will be shifted backwards since the frequency components at p are now at $p-1$. This is a circular shift, i.e., the frequency components at $p=-T+1$ will be moved to $p=T$. Moreover, the oldest frequency components that are now at $p=T$ are supposed to leave the window, and thus, be removed. Also, the new frequency components for the new sample that is entering the window should be added in front of the window. Finally, the effect of the most recent computed filter output at $t-1$ should be applied to $\mathcal{S}_{\mathbf{h}_1(t)}$. Using Theorem 1 in [13], $\mathcal{S}_{\mathbf{h}_1(t-1)}$ after a circular shift can be expressed as

$$\mathcal{R}_{\mathbf{h}_1(t-1)}=\mathbf{I}_{-1}\mathcal{S}_{\mathbf{h}_1(t-1)}\mathbf{E} \quad (37)$$

where $\mathbf{E}$ is a diagonal matrix whose nth diagonal element is $e^{\frac{j2\pi n}{N}}$ and

$$\mathbf{I}_{-1}=\left(\begin{array}{c|c}\mathbf{0}_{(2T-1)\times 1} & \mathbf{I}_{(2T-1)\times(2T-1)}\\ \hline 1 & \mathbf{0}_{1\times(2T-1)}\end{array}\right). \quad (38)$$

Then, the S-transform at t can be found as

$$\mathcal{S}_{\mathbf{h}_1(t)}=\ \mathcal{R}_{\mathbf{h}_1(t-1)}+[g(t+T)-(g(t-T)$$
$$-y(t-T))]\mathcal{S}_{\delta(x-T)}-y(t-1)\mathcal{S}_{\delta(x+1)}. \quad (39)$$

Likewise, the S-transform of the window form $t-2T-1$ to $t-1$, used to build the prototype, can be updated as

$$\mathcal{S}_{\mathbf{h}(t-T-1)}=\mathcal{R}_{\mathbf{h}(t-T-2)}+[(g(t-1)-y(t-1))$$
$$-(g(t-2T-2)-y(t-2T-2))]\mathcal{S}_{\delta(x-T)} \quad (40)$$

where

$$\mathcal{R}_{\mathbf{h}(t-T-2)}=\mathbf{I}_{-1}\mathcal{S}_{\mathbf{h}(t-T-2)}\mathbf{E}. \quad (41)$$

ACKNOWLEDGMENT

The authors would like to thank Dr. K. Gunnerson for his feedbacks and medical advising as the PI for the project IRB.The procedures followed in this work for data collection from human subjects were in accordance with the ethical standards of the Institutional Review Board on human experimentation (IRB number HM11963).

REFERENCES

[1] G. Cañadas, C. Dell'Aquila, and E. Laciar, "Development of portable device to measure respiratory activity based on impedance pneumography," in *II Latin American Conference on Bioimpedance*, vol. 54. New York, NY, USA: Springer, 2016, pp. 60–63.

[2] L. Poupard, M. Mathieu, M. Goldman, F. Chouchou, and F. Roche, "Multimodal ECG Holter system for sleep-disordered breathing screening," *Sleep Breathing*, vol. 16, no. 3, pp. 685–693, 2012.

[3] C. Rotariu, H. Costin, R. Ciobotariu, A. Păsărică, and C. Cristea, "Real-time system for continuous and remote monitoring of respiration during sleep using wireless sensors networks," in *International Conference on Advancements of Medicine and Health Care Through Technology; 5th–7th June 2014, Cluj-Napoca, Romania*. New York, NY, USA: Springer, 2014, pp. 83–86.

[4] M. C. Mlynczak, W. Niewiadomski, M. Zylinski, and G. P. Cybulski, "Ambulatory impedance pneumography device for quantitative monitoring of volumetric parameters in respiratory and cardiac applications," in *Proc. Comput. Cardiol. Conf.*, 2014, pp. 965–968.

[5] T. Vuorela, V.-P. Seppä, J. Vanhala, and J. Hyttinen, "Design and implementation of a portable long-term physiological signal recorder," *IEEE Trans. Inf. Technol. Biomed.*, vol. 14, no. 3, pp. 718–725, May 2010.

[6] M. H. Sim *et al.*, "Development and evaluation of an improved technique for pulmonary function testing using electrical impedance pneumography intended for the diagnosis of chronic obstructive pulmonary disease patients," *Sensors*, vol. 13, no. 11, pp. 15 846–15 860, 2013.

[7] V.-P. Seppä, M. Uitto, and J. Viik, "Tidal breathing flow-volume curves with impedance pneumography during expiratory loading," in *Proc. IEEE 35th Annu. Int. Conf. Eng. Med. Biol. Soc.*, 2013, pp. 2437–2440.

[8] V.-P. Seppä, A. S. Pelkonen, A. Kotaniemi-Syrjänen, M. J. Mäkelä, J. Viik, and L. P. Malmberg, "Tidal breathing flow measurement in awake young children by using impedance pneumography," *J. Appl. Physiol.*, vol. 115, no. 11, pp. 1725–1731, 2013.

[9] V.-P. Seppä, J. Viik, and J. Hyttinen, "Assessment of pulmonary flow using impedance pneumography," *IEEE Trans. Biomed. Eng.*, vol. 57, no. 9, pp. 2277–2285, Sep. 2010.
[10] M. Młyńczak, W. Niewiadomski, M. Żyliński, and G. Cybulski, "Verification of the respiratory parameters derived from impedance pneumography during normal and deep breathing in three body postures," in *6th European Conference of the International Federation for Medical and Biological Engineering*. New York, NY, USA: Springer, 2015, pp. 881–884.
[11] N. Khambete, B. Brown, and R. Smallwood, "Movement artefact rejection in impedance pneumography using six strategically placed electrodes," *Physiol. Meas.*, vol. 21, no. 1, pp. 79–88, 2000.
[12] M. Młyńczak and G. Cybulski, "Impedance pneumography: Is it possible?" in *Proc. Photon. Appl. Astronomy, Commun. Industry, High-Energy Phys. Exp.*, 2012, pp. 84 541T–84 541T.
[13] S. Ansari, K. Ward, and K. Najarian, "Epsilon-tube filtering: Reduction of high-amplitude motion artifacts from impedance plethysmography signal," *IEEE J. Biomed. Health Inform.*, vol. 19, no. 2, pp. 406–417, Mar. 2015.
[14] V. Vapnik. (1998). *Statistical Learning Theory* (Adaptive and learning systems for signal processing, communications, and control) [Online]. Wiley. Available: http://books.google.com/books?id=GowoAQAAMAAJ
[15] A. Sahakian, W. Tompkins, and J. Webster, "Electrode motion artifacts in electrical impedance pneumography," *IEEE Trans. Biomed. Eng.*, vol. BME-32, no. 6, pp. 448–451, Jun. 1985.
[16] S. Luo, V. Afonso, J. Webster, and W. Tompkins, "The electrode system in impedance-based ventilation measurement," *IEEE Trans. Biomed. Eng.*, vol. 39, no. 11, pp. 1130–1141, Nov. 1992.
[17] V.-P. Seppä, J. Hyttinen, M. Uitto, W. Chrapek, and J. Viik, "Novel electrode configuration for highly linear impedance pneumography," *Biomedizinische Technik/Biomed. Eng.*, vol. 58, no. 1, pp. 35–38, 2013.
[18] J. Rosell and J. Webster, "Signal-to-motion artifact ratio versus frequency for impedance pneumography," *IEEE Trans. Biomed. Eng.*, vol. 42, no. 3, pp. 321–323, Mar. 1995.
[19] J. Rosell, K. Cohen, and J. Webster, "Reduction of motion artifacts using a two-frequency impedance plethysmograph and adaptive filtering," *IEEE Trans. Biomed. Eng.*, vol. 42, no. 10, pp. 1044–1048, Oct. 1995.
[20] A. K. Barros, A. Mansour, and N. Ohnishi, "Removing artifacts from electrocardiographic signals using independent components analysis," *Neurocomputing*, vol. 22, no. 1, pp. 173–186, 1998.
[21] M. Chawla, "PCA and ICA processing methods for removal of artifacts and noise in electrocardiograms: A survey and comparison," *Appl. Soft Comput.*, vol. 11, no. 2, pp. 2216–2226, 2011.
[22] M. Milanesi, N. Martini, N. Vanello, V. Positano, M. Santarelli, and L. Landini, "Independent component analysis applied to the removal of motion artifacts from electrocardiographic signals," *Med. Biol. Eng. Comput.*, vol. 46, no. 3, pp. 251–261, 2008.
[23] M. Milanesi *et al.*, "Multichannel techniques for motion artifacts removal from electrocardiographic signals," in *Proc. IEEE 28th Annu. Eng. Med. Biol. Soc.*, 2006, pp. 3391–3394.
[24] B. S. Kim and S. K. Yoo, "Motion artifact reduction in photoplethysmography using independent component analysis," *IEEE Trans. Biomed. Eng.*, vol. 53, no. 3, pp. 566–568, Mar. 2006.
[25] P. S. Hamilton and M. G. Curley, "Adaptive removal of motion artifact [ECG recordings]," in *Proc. IEEE 19th Annu. Int. Conf. Eng. Med. Biol. Soc.*, vol. 1, 1997, pp. 297–299.
[26] P. Hamilton, M. Curley, R. Aimi, and C. Sae-Hau, "Comparison of methods for adaptive removal of motion artifact," in *Proc. Comput. Cardiol*, 2000, pp. 383–386.
[27] D. Jeong and S. Kim, "Development of a technique for cancelling motion artifact in ambulatory ECG monitoring system," in *Proc. 3rd Int. Conf. Convergence Hybrid Inform. Technol.*, vol. 1, 2008, pp. 954–961.
[28] D. Tong, K. Bartels, and K. Honeyager, "Adaptive reduction of motion artifact in the electrocardiogram," in *Proc. 2nd Joint 24th Annu. Conf. Eng. Med. Biol./Annu. Fall Meet. Biomed. Eng. Soc.*, vol. 2, 2002, pp. 1403–1404.
[29] S. Liu, "Motion artifact reduction in electrocardiogram using adaptive filter," *J. Med. Biol. Eng.*, vol. 31, no. 1, pp. 67–72, 2011.
[30] K. Chan and Y. Zhang, "Adaptive reduction of motion artifact from photoplethysmographic recordings using a variable step-size LMS filter," in *Proc. IEEE Sensors*, vol. 2, 2002, pp. 1343–1346.
[31] S. Luo and W. Tompkins, "Experimental study: Brachial motion artifact reduction in the ECG," in *Proc. Comput. Cardiol.*, 1995, pp. 33–36.
[32] M. Raya and L. Sison, "Adaptive noise cancelling of motion artifact in stress ECG signals using accelerometer," in *Proc. 2nd Joint 24th Annu. Conf. Eng. Med. Biol./Annu. Fall Meet. Biomed. Eng. Soc.*, vol. 2, 2002, pp. 1756–1757.
[33] H. H. Asada, H.-H. Jiang, and P. Gibbs, "Active noise cancellation using MEMS accelerometers for motion-tolerant wearable bio-sensors," in *Proc. IEEE 26th Annu. Int. Conf. Eng. Med. Biol. Soc.*, vol. 1., 2004, pp. 2157–2160.
[34] S. Yoon, S. Min, Y. Yun, S. Lee, and M. Lee, "Adaptive motion artifacts reduction using 3-axis accelerometer in E-textile ECG measurement system," *J. Med. Syst.*, vol. 32, no. 2, pp. 101–106, 2008.
[35] H. Han, M.-J. Kim, and J. Kim, "Development of real-time motion artifact reduction algorithm for a wearable photoplethysmography," in *Proc. IEEE 29th Annu. Int. Conf. Eng. Med. Biol. Soc.*, 2007, pp. 1538–1541.
[36] M. Ur Rahman, R. Shaik, and D. Reddy, "An efficient noise cancellation technique to remove noise from the ECG signal using normalized signed regressor LMS algorithm," in *IEEE Int. Conf. Bioinformat. Biomed.*, 2009, pp. 257–260.
[37] S. Seyedtabaii and L. Seyedtabaii, "Kalman filter based adaptive reduction of motion artifact from photoplethysmographic signal," *Proc. World Acad. Sci., Eng. Technol.*, vol. 27, 2008, pp. 173–176.
[38] B. Lee, J. Han, H. J. Baek, J. H. Shin, K. S. Park, and W. J. Yi, "Improved elimination of motion artifacts from a photoplethysmographic signal using a Kalman smoother with simultaneous accelerometry," *Physiol. Meas.*, vol. 31, no. 12, pp. 1585–1603, 2010.
[39] L. B. Wood and H. H. Asada, "Low variance adaptive filter for cancelling motion artifact in wearable photoplethysmogram sensor signals," in *Proc. IEEE 29th Annu. Int. Conf. Eng. Med. Biol. Soc.*, 2007, pp. 652–655.
[40] K. A. Reddy and V. J. Kumar, "Motion artifact reduction in photoplethysmographic signals using singular value decomposition," in *Proc. IEEE Inst. Meas. Technol. Conf.*, 2007, pp. 1–4.
[41] K. A. Reddy, B. George, and V. J. Kumar, "Use of Fourier series analysis for motion artifact reduction and data compression of photoplethysmographic signals," *IEEE Trans. Inst. Meas.*, vol. 58, no. 5, pp. 1706–1711, May 2009.
[42] J. Lee, W. Jung, I. Kang, Y. Kim, and G. Lee, "Design of filter to reject motion artifact of pulse oximetry," *Comput. Standards Interfaces*, vol. 26, no. 3, pp. 241–249, 2004.
[43] Y. Yong-sheng, P. C. CY, and Z. Yuan-ting, "Reduction of motion artifact in pulse oximetry by smoothed pseudo Wigner-Ville distribution," *J. NeuroEng. Rehabil.*, vol. 2, no. 3, p. 9, 2005.
[44] C. Lee and Y. Zhang, "Reduction of motion artifacts from photoplethysmographic recordings using a wavelet denoising approach," in *Proc. IEEE EMBS Asian-Pacific Conf. Biomed. Eng.* 2003, pp. 194–195.
[45] S. Ansari, K. Ward, and K. Najarian, "ε-tube regression: A new method for motion artifact reduction," in *Proc. Annu. Int. Conf. Eng. Med. Biol. Soc.*, 2011, pp. 2736–2739.
[46] R. Stockwell, L. Mansinha, and R. Lowe, "Localization of the complex spectrum: The S transform," *IEEE Trans. Signal Process.*, vol. 44, no. 4, pp. 998–1001, Apr. 1996.
[47] J. B. Rosen, "The gradient projection method for nonlinear programming. Part I. Linear constraints," *J. Soc. Ind. Appl. Math.*, vol. 8, no. 1, pp. 181–217, 1960.
[48] K. T. Sweeney, T. E. Ward, and S. F. McLoone, "Artifact removal in physiological signals—Practices and possibilities," *IEEE Trans. Inform. Technol. Biomed.*, vol. 16, no. 3, pp. 488–500, May 2012.

Sardar Ansari (M'09) received the Bachelors degree in software engineering from the Electrical and Computer Engineering Department, University of Tehran, Tehran, Iran, in 2008, the M.S. degree in computer science from Virginia Commonwealth University (VCU), Richmond, VA, USA, in 2010, and the M.S. degree in statistics and the Ph.D. degree in computer science from VCU in 2013.

He is a Research Fellow in the Department of Emergency Medicine, University of Michigan, Ann Arbor, MI, USA and a Member of Michigan Center for Integrative Research in Clinical Care. His research interests include medical signal and image processing, machine learning, data mining, and development of medical devices as well as nonlinear and discrete optimization and queuing theory.

Kevin R. Ward received the B.S. degree in physiology from Louisiana State University in Baton Rouge and his degree in medicine from Tulane University in New Orleans, LA, USA. He then completed a residency in Emergency Medicine at the University of Pittsburgh, USA.

He is a Professor in the Department of Emergency Medicine, University of Michigan, Ann Arbor, MI, USA. He is an Instrumental Member of the Michigan Critical Injury and Illness Research Center. He has published more than 200 peer-reviewed articles, abstracts, and chapters. His research interests include developing a broad platform technologies for the diagnosis, monitoring, and treatment of the critically injured including a focus on combat casualty care.

Dr. Ward received many awards including the Peter Safar Award in Graduate Research from the University of Pittsburgh, the Society of Academic Emergency Medicine's Young Investigator Award, and the U.S Army's Advanced Technologies Applications in Combat Casualty Care Award. He is also a prolific inventor and received the 2010 Virginia Commonwealth University Billie Martin Innovator of the Year Award.

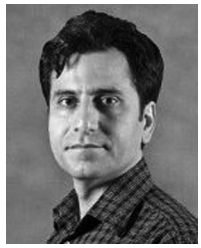

Kayvan Najarian (SM'07) received the B.Sc. degree in electrical engineering from Sharif University, Tehran, Iran, the M.Sc. degree in biomedical engineering from Amirkabir University, Tehran, and the Ph.D. degree in electrical and computer engineering from the University of British Columbia, Vancouver, Canada.

He is an Associate Professor in the Departments of Computational Medicine and Bioinformatics, and Emergency Medicine, University of Michigan, Ann Arbor, MI, USA. He also serves as the Director of the Michigan Center for Integrative Research in Critical Care's Biosignal-Image and Computational (BIC) Core program. His research interests include the design of signal/image processing and machine learning methods to create computer-assisted clinical decision support systems that improve patient care.

Dr. Najarian serves as the Editor-in-Chief of a journal in the field of biomedical engineering as well as the Associate Editor of two journals in the field of biomedical informatics. He is also a Member of many editorial boards and has served as a Guest Editor of special issues for several journals.